Thermochemical Sulphate Reduction Can Improve Carbonate Petroleum Reservoir Quality

Lei Jiang[1,2,3,4*], Richard H Worden[5], Changbing Yang[3]

[1]Key Laboratory of Petroleum Resources Research, Institute of Geology and Geophysics, Chinese Academy of Sciences, Beijing 100029, China (email: lei.jiang@mail.iggcas.ac.cn)

[2]Institutions of Earth Science, Chinese Academy of Sciences, Beijing 100029, China

[3]Bureau of Economic Geology, Jackson School of Geosciences, The University of Texas at Austin, Austin, TX 78713, USA

[4]Department of Geology and Geophysics, Yale University, New Haven, CT 06511, USA

[5]Department of Earth, Ocean and Ecological Sciences, University of Liverpool, 4 Brownlow Street, Liverpool, L69 3GP, UK

Abstract

Interest in the creation of secondary pore space in petroleum reservoirs has increased because of a need to understand deeper and more complex reservoirs. The creation of new secondary porosity that enhances overall reservoir quality in deeply buried carbonate reservoirs is controversial and some recent studies have concluded it is not an important phenomenon. Here we present petrography, geochemistry, fluid inclusion data, and fluid-rock interaction reaction modeling results from Triassic Feixianguan Formation, Sichuan Basin, China, core samples and explore the relative importance of secondary porosity due to thermochemical sulphate reduction (TSR)

during deep burial diagenesis. We find that new secondary pores result from the dissolution of anhydrite and possibly from dissolution of the matrix dolomite. Assuming porosity before TSR was 16 % and the percentage of anhydrite was 6 %, modelling shows that, due to TSR, 1.6 % additional porosity was created that led to permeability increasing from 110 mD (range 72 to 168 mD within a 95% confidence interval) to 264 mD (range 162 to 432 mD within a 95 % confidence interval). Secondary porosity results from the density differences between reactant anhydrite and product calcite, the addition of new water during TSR, and the generation of acidity during the reaction of new H_2S with the siderite component in pre-existing dolomite in the reservoir. Fluid pressure was high during TSR, and approached lithostatic pressure in some samples; this transient overpressure may have led to the maintenance of porosity due to the inhibition of compactional processes. An additional 1.6 % porosity is significant for reserve calculations, especially considering that it occurs in conjunction with elevated permeability that results in faster flow rates to the production wells.

Keywords: Mesogenetic dissolution, thermochemical sulphate reduction, carbonate reservoir, fluid inclusion, fluid pressure.

Introduction

Thermochemical sulphate reduction (TSR) is the abiological oxidation of hydrocarbons by sulphate (due to the dissolution of anhydrite, celestite and barite in sedimentary basins) at elevated temperatures, typically higher than 110 ºC (Jiang et al., 2015c; Machel, 2001; Worden et al., 1995). Significant alteration of petroleum, generation of reduced forms of sulphur (S and H_2S), and oxidized forms of carbon

(carbonate minerals and CO_2) are typically the results of TSR. TSR can also generate water, metal sulphides, organosulphur compounds, and bitumen (Bildstein et al., 2001; Cai et al., 2003; Jiang et al., 2015c; Machel, 1987; Machel et al., 1995; Worden et al., 2000; Worden et al., 1995).

A general reaction summarizing TSR:

$$\text{sulphate+ petroleum} \rightarrow \text{calcite} + H_2S \pm H_2O \pm CO_2 \pm S \pm \text{altered petroleum} \quad (1)$$

Simple stoichiometric TSR reactions in many sedimentary basins (e.g. Feixianguan Formation, Sichuan Basin; Khuff Formation, Abu Dhabi; Upper Devonian and Mississippian strata, Alberta, Canada) between anhydrite and the two simplest hydrocarbons:

$$CaSO_4 + CH_4 \rightarrow CaCO_3 + H_2S + H_2O \quad (2)$$

$$2CaSO_4 + C_2H_6 \rightarrow 2CaCO_3 + H_2S + 2H_2O + S \quad (3)$$

$$7CaSO_4 + 4C_2H_6 \rightarrow 7CaCO_3 + 7H_2S + 5H_2O + CO_2 \quad (4)$$

Most TSR-related studies have focused on stable isotope geochemistry and the geochemistry of petroleum, sulphate, and the products of TSR (e.g. CO_2, H_2S, S), and few focus on the ability of TSR to form new pore spaces in deeply buried rocks and thus improve carbonate reservoirs quality. For example, it is proposed that deep burial diagenesis in a closed system (including TSR) is not able to enhance porosity and permeability in carbonate reservoirs (Ehrenberg et al., 2012; Heydari, 1997; Machel and Buschkuehle, 2008). In the Upper Jurassic Smackover Formation, Mississippi, TSR appears to have resulted in large amount of calcite precipitation with significant porosity-loss (Heydari, 1997). Carbonate reservoirs in the Southesk-Cairn Carbonate

71 Complex (SCCC), Alberta Basin, indicate the overall change of porosity and
72 permeability during TSR is small. Similarly, based on a literature review and
73 modelling, Ehrenberg et al. (2012) suggested that mesogenetic dissolution, producing
74 a net increase in secondary porosity, is not likely during deep burial diagenesis. By
75 contrast, detailed petrographic, geochemical, and modelling work (TSR impact on the
76 carbonate reservoir quality) from the Western Canada Sedimentary Basin (WCSB)
77 determined that while 75% of the porosity created by dissolution of anhydrite during
78 TSR was lost due to calcite precipitation, net porosity increased 1 to 2% (Hutcheon
79 and Krouse, 1994; Hutcheon et al., 1995).

80 There is evidence for extensive TSR in the Feixianguan Formation, based on: (1)
81 coexistence of TSR calcite, elemental sulphur, pyrite, sulphur-enriched bitumen, and
82 anhydrite (Jiang et al., 2014a); (2) broad overlap of sulphur isotopes of TSR-
83 generated pyrite, elemental sulphur, sulphur in bitumen and H_2S, with values
84 approaching $\delta^{34}S$ value of the pre-existing, early diagenetic anhydrite that is
85 equivalent to coeval seawater sulphur isotopes (Cai et al., 2010; Hao et al., 2008; Zhu
86 et al., 2005); (3) relatively high fluid inclusion homogenization temperatures found in
87 TSR calcite (from ~110 ºC to 220 ºC) (Jiang et al., 2014a, 2015c), and; (4) gas
88 geochemical characteristics including: relatively high H_2S concentration (up to 58%)
89 that replaced the CH_4 in gas reservoirs, the extremely high gas dryness ($C_1/\sum C_n$)
90 (>0.95), positive relationship of gas souring index [$GIS = H_2S/(H_2S + \sum Cn)$] (Worden
91 et al., 1995) and TSR extent parameter [$CO_2/(CO_2 + \sum C_nH_{2n+2})$] (Krouse et al., 1988),
92 and the $\delta^{13}C$ values of methane and ethane with a different extent of TSR (Cai et al.,
93 2013; Hao et al., 2008; Li et al., 2005; Liu et al., 2013; Liu et al., 2014).

94 The Feixianguan Formation in the Sichuan Basin, China, offers an ideal place to study
95 the impact of TSR on deeply buried carbonate reservoir quality, because it was a
96 relatively closed diagenetic environment during TSR (Jiang et al., 2015a; Jiang et al.,
97 2015c). There is little evidence for diagenetic fluids (e.g., meteoric water,
98 hydrothermal fluids, deep basinal fluids) influencing the carbonate reservoir during
99 TSR. While a number of studies have focused on TSR in the Feixianguan Formation,
100 only two have investigated the impact of TSR on porosity: Cai et al. (2014) suggested
101 TSR was responsible for dissolution of dolomite and anhydrite with an overall
102 positive effect on dolostone reservoir quality; by contrast, Hao et al. (2015) suggested
103 TSR diagenesis was dominated by calcite cementation that reduced reservoir quality
104 in the Feixianguan Formation. This study will focus on resolving this conflict and
105 establishing the impact of TSR on carbonate reservoirs using the Feixianguan
106 Formation, by addressing the following questions:

107 1. Did new secondary pores develop in the Feixianguan Formation during TSR?

108 2. If secondary pores did form during TSR, what are their characteristics?

109 3. What are the possible mechanisms for enhanced reservoir quality during TSR?

110 To answer these questions, we focus on representative wells which have experienced
111 TSR by applying conventional core description techniques, point counting,
112 transmitted-light petrography, scanning electron microscope (SEM) petrography,
113 fluid-inclusion analysis and pressure modelling, and diagenesis modelling.

114 **Geological setting**

115 The diamond-shaped, intracratonic, 230,000 km^2 Sichuan Basin is located in the east
116 of Sichuan Province, southwest China (Fig. 1A). The Sichuan Basin is tectonically-

bounded by the Longmenshan fold belt in the northwest, the Micangshan uplift in the north, the Dabashan fold belt in the northeast, the Hubei-Hunan-Guizhou fold belt in the southeast, and by the Emeishan-Liangshan fold belt in the southwest (Fig. 1A).

The Lower Triassic Feixianguan Formation (T_1f) carbonates occupy high energy facies belts dominated by oolitic carbonates (Fig. 1B) (Ma et al., 2008a; Zhao et al., 2005). During deposition of the Feixianguan Formation, open to semi-restricted carbonate platforms, in an arid climate, with fluctuating sea level, resulted in deposition of oolitic shoals and multiple gypsiferous layers on the margins of Kaijiang-Liangping Bay. Towards the end of Feixianguan deposition, aridity increased and the platforms became more restricted, which resulted in multiple gypsum beds interlayered with thin-bedded micritic limestones (Fig. 2). These upper evaporitic layers provide the regional seal for the underlying carbonate reservoirs (Zhao et al., 2005).

Seawater evaporation from lagoons, on the restricted platform to platform margin, is reported to have caused the initial dolomitization in the Feixianguan Formation (Jiang et al., 2013; Jiang et al., 2014b; Zhao et al., 2005). The most significant dolomitization phase then occurred in shallow burial environments by reflux of mesohaline water or seawater dolomitization (Jiang et al., 2014b). The latest dolomitization event occurred during burial, at temperatures ranging from 80°C to 140°C, due to invasion of high salinity water, most likely from the overlying Jialingjiang Formation (Jiang et al., 2014b). The Feixianguan Formation on the NE side of the Kaijiang-Liangping Bay is more dolomitized compared to the SW side, perhaps because of local differences in aridity during deposition (Jiang et al., 2014b; Zhao et al., 2005).

Burial histories in the Sichuan Basin were dominated by rapid burial in the Triassic and early Jurassic to depths of ~7500 m and temperatures of 220°C followed by uplift prior to the Cretaceous Yanshan movement . This history has led to early Triassic gas reservoirs with temperatures between 100 and 140°C at the present day (Ma et al., 2008a). Thermochemical sulphate reduction (TSR) occurred during appropriate elevated temperature conditions, where there was sufficient supply of anhydrite and petroleum. The Feixianguan Formation carbonate has variable H_2S concentrations generally between 10% and 20%, but up to 60% in some reservoirs (Cai et al., 2013; Hao et al., 2008; Li et al., 2005; Liu et al., 2014).

Methods

More than 100 core samples were collected from the lower unit of the Triassic Feixianguan Formation from the Puguang, Luojiazhai, Dukouhe, Maoba and Jingzhu carbonate reservoir gas fields. These fields were chosen since they have variable degrees of gas sourness. Polished sections, and conventional thin sections that were stained with Alizarin Red S to distinguish calcite and dolomite, were prepared from all samples. Selected samples were examined by scanning electron microscope (SEM) in backscattered electron imaging mode (BSEM), and elemental analysis by energy dispersive X-ray spectroscopy (EDS). Point counting of the stained thin sections (500 points for each sample) was used to determine the mineral and pore-type proportions.

Fluid inclusion homogenization temperatures (T_h) and last ice melting temperatures (T_m) were measured from fluid inclusion assemblages (FIAs) containing two-phase aqueous inclusions in five doubly polished, detached (50 to 60 μm thick) wafers. The use of FIAs to determine temperatures of mineral growth, as opposed to single inclusions, provides confidence that the T_h data are credible and minimizes the effects

of artefacts, such as thermal re-equilibration (Goldstein, 2012; Goldstein and Reynolds, 1994). Fluid inclusion microthermometry was conducted using a Zeiss Axioskop 40A Pol light microscope with a Linkam THM600/TS90 heating and cooling stage. Last ice melting temperatures were converted to salinity using standard equations (Bodnar, 2003; Oakes et al., 1990).

Coexistence of two-phase aqueous and single-phase hydrocarbon inclusions indicates that fluid inclusions were trapped in the immiscible two-phase field, and measured aqueous inclusion homogenization temperatures thus represent trapping temperatures (Goldstein and Reynolds, 1994). Raman analysis was undertaken for individual hydrocarbon fluid inclusions using LabRAM ARAMIS equipment. The position of each measured Raman line was determined, after baseline correction, using parameters for Gaussian/Lorentzian peak fitting (Lin et al., 2007). The 2851.38 and 2972.44 cm^{-1} Ne lines (relative to the 514.529 nm Rayleigh line of the Ar ion laser, in air) were used for calibration. Concentrations of methane and trapping pressures were calculated following the equations of state for the CH_4 system and the H_2O-NaCl-CH_4 system (Duan and Mao, 2006; Duan, 1992), using the approach of Becker et al. (2010).

The aim of geochemical modelling in this study is to simulate the overall change in mineral assemblage volume (including dolomite, calcite, and anhydrite) by considering the reaction described in equation (2) during TSR. A similar modelling strategy to the 3D reactive transport presented by Fu et al. (2016) was applied in this study. In contrast to Fu's model, our geochemical model focuses on geochemical reactions without considering groundwater flow and solute transport during the TSR. This simplification renders fast computation. The US Geological Survey's computer

189 program PHREEQC and the database thermodynamic wateq4f.dat were used to
190 simulate equilibrium reactions for aqueous species (Parkhurst and Appelo, 2013).
191 Temperatures, pressures, and fluid compositions obtained from the fluid study were
192 used as input to the geochemical model (details in the supplemental input file). In
193 addition, the kinetic rates of TSR were obtained from the model presented by Fu et al.
194 (2016). Mineral proportions were derived from point counting of the thin-section
195 samples. The modelling results for volume changes in mineral compositions were
196 further used to estimate change in porosity following the similar method presented by
197 Yang et al. (2008) and (Xu et al., 2010).

198 Permeability modelling was achieved by obtained the equation of relationship
199 between porosity and permeability, which can be obtained from the measured core
200 plug petrophysical data. The changes of permeability during TSR were calculated by
201 inputting the modelled porosity change during TSR to the calculated porosity-
202 permeability relationship equation, using 95 % confidence limits to present ranges for
203 the derived permeability values.

204 **Results**

205 **Thermochemical sulphate reduction diagenetic minerals**

206 Dolomite crystal sizes typically range from 50 to 200 μm in Feixianguan Formation
207 sucrosic dolostone reservoirs (Fig. 3). Here we illustrate that late diagenetic TSR
208 calcite locally fills pores but is heterogeneously distributed in these dolostone
209 reservoirs, with some parts of the reservoir filled with calcite whereas other parts
210 contain open pores (Fig. 3A, C; Fig. 4B, D; Fig. 5C). Pore characteristics have been
211 strongly modified by diagenetic processes, with some pores occupied by diagenetic
212 minerals and some enlarged by carbonate dissolution (Fig. 3B, D; Figs. 4 and 5).

Calcite produced by TSR represents the most volumetric mineral during TSR (in contrast to elemental sulphur), with average point-counted volumes of 1.6 ± 3.4 % (N=44) and a maximum volume of up to 17 % (Table 1). Two types of TSR calcite have been identified: TSR calcite that contains oil or bitumen inclusions is here defined as oil-stage TSR calcite, and TSR calcite with no evidence of oil or bitumen inclusions is defined as gas-stage TSR calcite. These calcites may either have precipitated from fluids in open pores or replaced the former anhydrite cement within the reservoir (Jiang et al., 2014a).

Euhedral pyrite is locally present in pores either as replacement of dolomite or in pores that are also typically associated with elemental sulphur (Fig. 4A). The average point counted volume of pyrite is less than 0.4 ± 0.9 % (N=44) (Table 1). Elemental sulphur in dolostone reservoir is best shown using BSEM analysis and commonly occurs with pyrite and TSR calcite (Figs. 3, 4, and 5). The total point counted volume of sulphur is less than 0.1% (N=44) although it is locally enriched at the edges of dissolution-enlarged pores. Elemental sulphur is appears similar to bitumen in the optical microscope (opaque and irregular in form). Bitumen is commonly present as sheet- and sphere-shape masses, with length or diameter in a range from 10 to 100 μm (Figs. 3 and 5), and represents 4.4 ± 5.4 % (N=44) rock volume (Table 1).

Dissolution-enlarged pores

Pore spaces in the Feixianguan Formation are dominated by dissolution-enlarged pores, which are commonly associated with TSR calcite, elemental sulphur, pyrite and bitumen (Figs. 3 and 45). There are two main occurrences of dissolution-enlarged pores in the Feixianguan dolostone reservoirs. The first type is selective dissolution pores. These are represented either by solution-enhanced vugs, where moldic pores

have been enlarged, or by complete dissolution of anhydrite cement; these dissolution pores are relatively large (up to 2 mm) (Fig. 4; Fig. 5A, B). The second type is characterised by partial or complete dissolution of coarse crystalline dolomite (Fig. 5D). Elemental sulphur commonly occurs on the edges of dissolution pores but there is notably little TSR calcite present (Figs. 3 and 5). The point counted (meso) porosity for these good dolostone reservoirs is in the range from 0% to 33 %, average at 9.7 ± 7.5 % (N=44) (Table 1).

Fluid inclusion microthermometry

Calcite produced by TSR contains primary, two-phase aqueous inclusions. Fluid inclusion homogenization temperature (T_h) variations within fluid inclusion assemblages (FIAs) from TSR calcite are generally less than about 10 °C (Fig. 6). Salinity values, determined from last ice melting temperatures, vary from less than 5 wt % NaCl to nearly 25 wt % NaCl for TSR calcites.

Measured homogenization temperatures (T_h) for FIAs (and isolated fluid inclusions) for oil-dominated TSR calcite range from approximately 110 °C to 200 °C (Fig. 6). In contrast, gas-dominated TSR calcite has a T_h range from 135 °C to 210 °C (Fig. 6). The temperatures obtained from the inclusions in TSR calcite represent minimum trapping temperatures (Goldstein and Reynolds, 1994). Oil-stage TSR calcite has decreasing salinity with increasing temperature, while, in contrast, gas-stage TSR has decreasing salinity with decreasing temperature (Fig. 6). The T_h-salinity distribution defines a progressive evolution during burial and heating, initially in the presence of oil with ever-falling salinity, and then in the presence of gas once the oil underwent cracking at maximum burial, followed by uplift and cooling in the presence of the evolved gas charge (Fig. 6).

Methane concentrations of fluid inclusions and trapping pressures

Aqueous fluid inclusions in TSR calcite in the Feixianguan Formation have bulk methane concentrations over a wide range from ~ 1500 to 11000 ppm, corresponding to trapping pressures of ~ 25 to 165 MPa (Fig. 7). By reference to the large-scale thermal cycle revealed by the oil-stage TSR calcite and then the gas-stage TSR calcite (Fig. 6), it is possible to infer the pressure evolution of the Feixianguan Formation during TSR. The fluid inclusions show variations in pressure with temperature with a clear subdivision of the oil-stage and gas-stage TSR calcites. The increasing temperature for the oil-stage calcite reveals increasing fluid pressure with time (and with heating) as the Feixianguan Formation was buried to ~7000 m (temperature of ~220°C). The switch to gas-stage calcite at elevated temperature shows that uplift to the current burial depth of ~3000 to 5000 m (temperatures of ~ 120 to 140 °C) was accompanied by decreasing fluid pressure with time (and with cooling). The highest fluid pressures approach the simulated trapping pressures (153-160MPa) for high density methane inclusions reported elsewhere for the Feixianguan Formation (Liu et al., 2009). Fluid pressures approach, and exceed in some cases, the modelled lithostatic pressure gradient suggesting that at least some of the fractures present in these rocks maybe due to excess fluid pressure.

Thermochemical sulphate reduction modelling result

Prior to TSR, calcite and anhydrite are here interpreted to have been abundant minerals in the dolostone Feixianguan Formation reservoirs (representing 1 and 6 wt. %, respectively) with porosity of 16% (Table 2), based on the point count data. The gas phase in these reservoirs is dominated by CH_4 (95 vol. %), CO_2 (2 vol. %), and N_2 (1.5 vol. %). The initial composition of pore water before the onset of TSR in

the geochemical model has been calculated by equilibrating of seawater through evaporation to the salinity obtained from fluid inclusion data. Temperature in the geochemical model was varied from 120 to 200 °C, based on the fluid inclusion evidence (Fig. 6).

Relative changes in mineral volumes for anhydrite, calcite, and dolomite at the steady state, based on the PHREEQC modelling results, are listed in Table 2. Anhydrite is consumed due to TSR, resulting in decreasing solid rock volume by 312.4 cm^3 (6.00 % of the total rock volume), whereas carbonate minerals precipitated and increased the solid rock volume by 212.8 cm^3 due to calcite (4.05 % of the total rock volume) and 1.3 cm^3 rock volume due to dolomite (0 % of the total rock volume). Hence there was a 1.95 % increase in relative porosity equating to an absolute post-TSR porosity increase of 1.6 %.

Sensitivity modelling of initial porosity of 10 % before TSR was also conducted; the results show that porosity increased by 1.7 % due to TSR (Table 2).

Permeability modelling result

An equation of the relationship between porosity and permeability was calculated based on the core plug petrophysical data: $Y = 0.0166e^{0.5498X}$, $R^2 = 0.6489$ (where Y and X stands for mD-permeability and percentage porosity, respectively).

The modelled permeability changes during TSR in the most proper porosity change in Case 1 (16 to 17.6 % porosity-increase due to TSR) is from 110 mD (before TSR, with a range 72 to 168 mD within a 95% confidence interval) to 264 mD (after TSR with a range 162 to 432 mD within a 95% confidence interval). For case 2 (10 to 11.7 %

porosity-increase due to TSR) is from 4.1 mD (before TSR) to 10.3 mD (after TSR) (Table 3).

Discussion

Conditions during TSR calcite growth

Comparison of the homogenization temperatures and salinities reveals a distinct separation that also relates to the type of host TSR calcite (Fig. 6). Oil was present in the reservoir before gas became the dominant petroleum phase, so initial calcite growth started in the presence of both oil and high salinity waters (25 wt % NaCl). Formation water salinity decreased to about 9 wt % NaCl during increasing temperature as oil-induced TSR progressed. After the oil charge evolved to a gas charge at elevated temperature, uplift occurred accompanied by decreasing temperature; the salinity of the formation water continued to fall (to 5 wt % NaCl) at this stage. The increasing and then decreasing temperatures in TSR calcites from the Feixianguan Formation are due to burial and uplift rather than invasion and subsequent cooling of hydrothermal fluids, (Jiang et al., 2015a; Jiang et al., 2014a).

The measured homogenisation temperature data from TSR calcite (Fig. 6) have been related to the derived trapping pressures (Fig. 7B). A modelled lithostatic pressure gradient of 25.4 MPa/km was calculated for a depth-averaged rock density of 2.59 g/cm^3, using wireline log data from the Sichuan Basin. A modelled hydrostatic pressure gradient was calculated as 9.9 MPa/km, based on a water density of 1.02 g/cm^3. Depths for the lithostatic and hydrostatic pressure gradients have been converted into temperature assuming a geothermal gradient of 24 °C/km (Liu et al., 2016; Qiu et al., 2008). Broadly speaking, the calculated fluid inclusion trapping pressures at the time of TSR calcite growth represent pore-fluid pressures that were

significantly above the hydrostatic pressure gradient (Fig. 7B). Many of the pore-fluid pressure measurements are near lithostatic pressures; some of the low pressure-temperature points lie at, or just below, the hydrostatic gradient (Fig. 7B).

Impact of thermochemical sulphate reduction on reservoir quality

According to petrographic observations reported here, dissolution-enhanced pore spaces tend to be spatially-close to TSR-related diagenetic minerals (pyrite, elemental sulphur, calcite) (Figs. 3 and 45). The close spatial association suggests that this secondary porosity, with point counted porosity values up to 32 % in one thin-section, formed by TSR. Our modelling work (Table 2) suggests that a porosity gain of 1.6 % is a consequence of TSR in the Feixianguan Formation, mainly due to the dissolution of anhydrite cement and/or nodules (Jiang et al., 2014b). This is different from the TSR modelling by Fu et al. (2016), within which the sulphate for TSR was derived from anhydrite seal, and porosity should be decreased by TSR-calcite precipitation in their model. Note that Hao et al. (2015) suggested, instead, that calcite cementation, rather than anhydrite and carbonate dissolution, dominated TSR diagenesis in the Feixianguan Formation, leading to porosity-*loss* during TSR. Our petrographic observations lead to a different conclusion. Porosity related to TSR dissolution has likely been underestimated by Hao et al. (2015) because they did not provide a detailed paragenetic sequence and also failed to discriminate TSR calcite from other types of diagenetic calcite. The diagenetic environments, reactants and products of TSR, and the gas geochemistry characteristics of the Feixianguan Formation are similar to those in the Western Canada Sedimentary Basin (Cai et al., 2014; Hao et al., 2008; Hutcheon et al., 1995; Jiang et al., 2015c; Zhu et al., 2005). Significantly, TSR modelling of the Western Canada Sedimentary Basin, by Hutcheon et al. (1995), also

showed that TSR probably led to an increase in porosity by 1 to 2 %, concurring with model outputs from the Feixianguan Formation. The permeability modelling result suggests that a net porosity increased from 1.6 % to 1.7 % by TSR, which doubled the reservoir permeability (Table 3), thus resulting in significantly enhancement of reservoir deliverability.

Elemental sulphur and calcite produced by TSR, as well as the TSR by-product pyrite, , typically occur at the edge of dissolution enlarged pores (Figs. 3 and 5). Elemental sulphur is routinely present in appreciable quantities in sour gas and oil reservoirs in the Arabian Gulf region and United Arab Emirates (Abou-Kassem, 2000), as well as in the Smackover Formation in southern Mississippi (Kuo, 1972). The freezing point of elemental sulphur, at atmospheric pressure, is 119 °C. Elemental sulphur and H_2S are miscible at high pressure allowing dissolution of H_2S into the liquid sulphur phase, and vice versa. Hence, it is likely that elemental sulphur is present as a liquid (or is dissolved in H_2S-rich gas) under reservoir temperatures and pressures conditions during and after TSR (Meyer, 1976). Elemental sulphur in the Feixianguan Formation may have been present either at the contact between local (pore-scale) oil-water or gas-water contacts with the host dolomites in the dissolution enlarged pores, possibly inhibiting calcite growth on surface of dolomite crystals (Fig. 3D; Fig. 5).

Pyrite was formed during TSR either via equation (5) or via equation (6) in the Feixianguan Formation (Fig. 4A) (Jiang et al., 2014a; Liu et al., 2013).

$$Fe^{2+} + 2H_2S \rightarrow FeS_2 + 4H^+ \quad (5)$$

$$FeCO_3 + 2H_2S \rightarrow FeS_2 + CO_2 + H_2O + H_2 \quad (6)$$

$$CaMg(CO_3)_2 + 4H^+ \rightarrow Ca^{2+} + Mg^{2+} + 2H_2O + 2CO_2 \quad (7)$$

For equation (6), we are not suggesting that pure siderite ($FeCO_3$) was present in the rock,rather that this represents the ferroan-component in dolomite, with iron likely being originally sourced from anoxic dolomitizing fluids. Point counted volumes of pyrite in the Feixianguan Formation range from 0 to 4 % (average of 0.4 %). Hence, at least near to the site of pyrite precipitation-- equation (5), the acidity of diagenetic fluids must have been increased by the release of H^+. As a consequence, carbonate dissolution is likely to have occurred, via equation (7), during and after pyrite precipitation in the Feixianguan Formation as a result of acid-creating equation (5) or via equation (6). Our modelling results show that TSR processes have not changed the volume of dolomite in these reservoirs (Table 2), although dolomite dissolution occurred after TSR. As mentioned above, this is consistent with isotopically-heavy CO_2 found in the Feixianguan Formation. Calcite produced by TSR has not been observed in direct association with pyrite and elemental sulphur in the Feixianguan Formation suggests that the slow rate of diffusion exceeds the rate of TSR. This may also suggest that the components required to make TSR calcite may have been transported away from the immediate reaction site and TSR in porous carbonates may be able to proceed more efficiently than TSR in a finely crystalline dolomite matrix (with low porosity and low permeability) (Jiang et al., 2014a; Worden et al., 2000). Calcite precipitation rates are slower than pyrite precipitation rates (Fu et al., 2016), and therefore it is possible that TSR calcite has been transported into other parts of the Feixianguan dolostone reservoirs via diffusion, fractures and/or faults formed by local tectonic movements, whereas pyrite growth may have occurred close to the original TSR site (Ma et al., 2008b). Although precipitation of 0.4% TSR-derived pyrite may have reduced porosity, the data presented here also shows that advanced carbonate

403 dissolution occurred as a result of pyrite precipitation. Hence, it is possible that the
404 overall effects of TSR-related pyrite precipitation and carbonate dissolution on these
405 dolostone reservoirs are positive in terms of reservoir quality.

406 **TSR impact on reservoir fluid composition and pressure**

407 According to balanced TSR equations (1-4), fluid phase H_2S, CO_2, elemental sulphur
408 and H_2O are all produced during TSR. Hence, both pore-fluid pressure and fluid
409 composition were significantly altered by TSR. Trace elements, rare earth elements,
410 and strontium isotopic data from TSR calcite demonstrate that TSR diagenesis most
411 likely represents a relatively closed system in the Feixianguan Formation (Jiang et al.,
412 2015a). Previously published oxygen isotope data from TSR calcite in the
413 Feixianguan Formation suggest that TSR-calcite precipitated in isotopic and thermal
414 equilibrium with the host rock, TSR water and sulphate minerals, and the negative
415 shift of carbon isotopes in this type of calcite is indicative of carbon partially sourced
416 from hydrocarbons due to TSR and partial adoption of the matrix dolomite $\delta^{13}C$
417 signal (Cai et al., 2014; Huang et al., 2012; Jiang et al., 2015c) similar to the
418 explanation of mixed $\delta^{13}C$ values in TSR calcite for other formations (Worden and
419 Smalley, 1996).

420 Fluid inclusion data show that about four times the volume of fresh water, compared
421 to the initial residual formation water, was generated by TSR and added to the fluids
422 in the Feixianguan Formation during TSR (Fig. 6) (Jiang et al., 2015c). Similar
423 findings have also been reported for the Permian Khuff Formation from Abu Dhabi
424 (Worden et al., 1996), and in the Devonian fields from the Western Canada
425 Sedimentary Basin (Yang et al., 2001). Generation of low salinity water by TSR
426 possibly resulted in the formation water being transiently undersaturated with respect

to calcite and dolomite, which would also facilitating the dissolution of carbonate minerals in the Feixianguan Formation.

The contact relationships of the ooids demonstrate that there is lack of compaction in these dolostone reservoirs, precluding the possibility that disequilibrium compaction contributed to the overpressure during progressive burial (Heydari, 2000). Therefore, the elevated fluid pressure (near lithostatic pressure) at maximum burial and the continuation of these high pressures during early uplift stage were probably related to the addition of gas either by oil cracking or TSR. It is possible that systematic increase in fluid overpressure during burial (Fig. 7B) was related to the generation of hydrocarbon gases due to secondary cracking of the primary oil that was originally derived from Upper Permian marine source rocks (Cai et al., 2010; Hao et al., 2008). Thermochemical sulphate reduction seems to have occurred simultaneously with oil cracking and had a significant impact on both gas composition and isotopes (Cai et al., 2013; Hao et al., 2008). An increase of fluid pressure due to the production of H_2S and CO_2 in these dolostone reservoirs (equation 4) has been proven to be a result of TSR (Liu et al., 2006). However, fluid pressure progressively decreased to near-hydrostatic pressure (~56 MPa) during further uplift (Fig. 7A)(Liu et al., 2009). Fluid pressure increasing during burial followed by a decreasing trend during uplifting demonstrates that oil cracking may have been completed from the maximum burial to early uplift stage, and continuation of exhumation and the generation of fractures may have released some fluid pressure in these dolostone reservoirs.

We propose a model in which oil cracking due to progressive burial and increasing temperature, associated with TSR, led to increasing pore-fluid pressure in the Feixianguan Formation. During uplift, after oil cracking and bitumen formation, TSR

continued to occur and produced H_2S and CO_2, maintaining some of the fluid pressure in the reservoir. In addition, pressure may have been episodically released from the system during uplift, resulting in methane exsolving from pore water into free-gas phase, maintaining methane saturation in the aqueous phase (Becker et al., 2010). Overpressure during TSR diagenesis may have resulted in the forcing of pore-fluids out of the TSR site. It is possible that a complex cycling of fluids on a reservoir scale is involved during TSR, resulting in some zones of reservoir develop higher porosity whereas others are occupied by calcite cements.

Implications for deeply buried carbonate reservoir exploration

In carbonate reservoirs, open system diagenesis, that can lead to enhanced porosity, has been proposed by numerous authors. In some carbonate systems, secondary porosity has been interpreted to have formed by near-surface karstification (Loucks, 1999), due to early dissolution by meteoric water and/or dolomitization during water leaching (Dickson and Kenter, 2014; Jiang et al., 2016; Lucia et al., 1994; Zhu et al., 2006), by mesogenetic dissolution (Kenter et al., 2006; Mazzullo and Harris, 1992), as well as by hydrothermal karstification and dissolution (Biehl et al., 2016a; Davies and Smith, 2006; Jiang et al., 2015b; Packard et al., 2001; Saller and Dickson, 2011; Smith, 2006). In contrast, in a closed or semi-closed burial diagenetic system, where water/rock ratios is low, the formation waters are commonly interpreted to be saturated with respect to calcite (Bjørlykke and Jahren, 2012; Ehrenberg et al., 2012).

Based on detailed petrographic and geochemical data, as well as permeability, pressure and geochemical modelling, we here conclude that porosity and permeability has been increased by TSR in the Feixianguan Formation even though this rock unit is probably part of a relatively closed system. The current CO_2 concentration measured

in the dolostone reservoir appears to correlate with H_2S concentrations, and carbon isotopic composition of the contemporary CO_2 gas is ^{13}C-enriched and does not reflect a ^{12}C-rich CO_2 that would be expected from oxidation of hydrocarbon by sulphate (Cai et al., 2014; Hao et al., 2015; Huang et al., 2012). This observation is consistent with significant dissolution occurring and ^{13}C-rich CO_2 added to these reservoirs. Carbonate dissolution during deep burial environments may be related to TSR by generation of water, supported by this study, TSR modelling (Fu et al., 2016), and generation of acidity during the reaction of H_2S with siderite component in dolomite. In addition, elemental sulphur generated by TSR may have maintained porosity from calcite precipitation. It is likely that TSR is capable of increasing reservoir heterogeneity and maintaining porosity by the inhibition of compactional processes due to the high fluid pressure conditions. Our study shows that TSR has enhanced the reservoir porosity by 1.6 % (Table 2) and doubled the permeability in the Feixianguan Formation dolostone (Table 3), which has clear and significant implications for petroleum exploration in deep sedimentary basins that experienced TSR (Biehl et al., 2016a; Biehl et al., 2016b; Bjørlykke and Jahren, 2012; Cai et al., 2014; Ehrenberg et al., 2012; Heydari, 1997; Jiang et al., 2015c; Machel and Buschkuehle, 2008; Mazzullo and Harris, 1991; Worden et al., 1996; Yang et al., 2001).

Conclusions

1. Deeply buried Feixianguan Formation dolostone reservoirs from the Sichuan Basin (mainly between 3000 and 6000 m) contain dissolution enlarged pore spaces. These dissolution pores have close genetic links to thermochemical sulphate reduction (TSR), suggesting that TSR was responsible for the enhancement of reservoir quality.

This is in agreement with geochemical model results that demonstrate an overall porosity increase of 1.6% and doubled permeability.

2. Elemental sulphur occurred as a liquid (or was dissolved in gas) present at the contact between petroleum and water or directly in contact with the host dolomites in the dissolution pores, inhibiting the new secondary pores from undergoing calcite precipitation.

3. Creation of fresh water under deep burial environments may cause dissolution of carbonate minerals because the formation water may become transiently undersaturated with respect to calcite and dolomite.

4. Overpressure caused complex cycling of fluids within the reservoir during TSR, resulting in some reservoir zones being occupied by calcite cements and others developing higher porosity, thus increasing reservoir heterogeneity.

5. Further dissolution of carbonate probably occurred because of the release of H^+ due to pyrite precipitation, with Fe sourced from a ferroan carbonate component in dolomite. This is supported by the positive $\delta^{13}C$ values of present-day CO_2 in these reservoirs.

6. This is the first documented case of how TSR can improve carbonate reservoir quality under a relatively closed diagenetic system. This phenomenon seems not to have been fully appreciated in other sedimentary basins that experienced TSR.

ACKNOWLEDGEMENTS:

This work has been financially supported by the Natural Science Foundation of China (Grant No. 41402132), the National Science and Technology Majoy Project (Grant No. 2017ZX05008-004), and scholarships under the China Postdoctoral Science Foundation award for International Postdoctoral Exchange Fellowship Program

(Grant No. 20150035) and the Chinese Scholarship Council (CSC) (Grant No. 201704910007).

References

Abou-Kassem, J.H. (2000) Experimental and numerical modeling of sulfur plugging in carbonate reservoirs. Journal of Petroleum Science and Engineering 26, 91-103.

Becker, S., Eichhubl, P., Laubach, S., Reed, R., Lander, R. and Bodnar, R. (2010) A 48 my history of fracture opening, temperature, and fluid pressure: Cretaceous Travis Peak Formation, East Texas basin. Geological Society of America Bulletin 122, 1081-1093.

Biehl, B.C., Reuning, L., Schoenherr, J., Lüders, V. and Kukla, P.A. (2016a) Impacts of hydrothermal dolomitization and thermochemical sulfate reduction on secondary porosity creation in deeply buried carbonates: A case study from the Lower Saxony Basin, northwest Germany. AAPG Bulletin 100, 597-621.

Biehl, B.C., Reuning, L., Schoenherr, J., Lewin, A., Leupold, M. and Kukla, P.A. (2016b) Do CO_2-charged fluids contribute to secondary porosity creation in deeply buried carbonates? Marine and Petroleum Geology 76, 176-186.

Bildstein, O., Worden, R.H. and Brosse, E. (2001) Assessment of anhydrite dissolution as the rate-limiting step during thermochemical sulfate reduction. Chemical Geology 176, 173-189.

Bjørlykke, K. and Jahren, J. (2012) Open or closed geochemical systems during diagenesis in sedimentary basins: Constraints on mass transfer during diagenesis and the prediction of porosity in sandstone and carbonate reservoirs. American Association of Petroleum Geologists, Bulletin 96, 2193-2214.

Bodnar, R.J. (2003) Reequilibration of fluid inclusions. Fluid inclusions: Analysis and interpretation 32, 213-230.

Cai, C.F., He, W.X., Jiang, L., Li, K.K., Xiang, L. and Jia, L.Q. (2014) Petrological and geochemical constraints on porosity difference between Lower Triassic sour-and sweet-gas carbonate reservoirs in the Sichuan Basin. Marine and Petroleum Geology 56, 34-50.

Cai, C.F., Li, K.K., Zhu, Y.M., Xiang, L. and Jiang, L. (2010) TSR origin of sulfur in Permian and Triassic reservoir bitumen, East Sichuan Basin, China. Organic Geochemistry.

Cai, C.F., Worden, R.H., Bottrell, S.H., Wang, L.S. and Yang, C.C. (2003) Thermochemical sulphate reduction and the generation of hydrogen sulphide and thiols (mercaptans) in Triassic carbonate reservoirs from the Sichuan Basin, China. Chemical Geology 202, 39-57.

Cai, C.F., Zhang, C.M., He, H. and Tang, Y.J. (2013) Carbon isotope fractionation during methane-dominated TSR in East Sichuan Basin gasfields, China: A review. Marine and Petroleum Geology 48, 100-110.

Davies, G.R. and Smith, L.B. (2006) Structurally controlled hydrothermal dolomite reservoir facies: An overview. American Association of Petroleum Geologists, Bulletin 90, 1641.

Dickson, J.A.D. and Kenter, J.A.M. (2014) Diagenetic Evolution of Selected Parasequences Across A Carbonate Platform: Late Paleozoic, Tengiz Reservoir, Kazakhstan. Journal of Sedimentary Research 84, 664-693.

Duan, Z. and Mao, S. (2006) A thermodynamic model for calculating methane solubility, density and gas phase composition of methane-bearing aqueous fluids from 273 to 523K and from 1 to 2000bar. Geochimica et Cosmochimica Acta 70, 3369-3386.

Duan, Z.H. (1992) An equation of state for the C&-CO*-Hz0 system: II. Mixtures from 50 to 1000 C and 0 to 1000 bar.

572 Ehrenberg, S.N., Walderhaug, O. and Bjørlykke, K. (2012) Carbonate porosity creation by
573 mesogenetic dissolution: Reality or illusion? American Association of Petroleum
574 Geologists, Bulletin 96, 217-233.
575 Fu, Y.J., van Berk, W. and Schulz, H.-M. (2016) Hydrogen sulfide formation, fate, and
576 behavior in anhydrite-sealed carbonate gas reservoirs: A three-dimensional reactive
577 mass transport modeling approach. American Association of Petroleum Geologists,
578 Bulletin 100, 843-865.
579 Goldstein, R.H. (2012) Fluid inclusion geothermometry in sedimentary systems: from
580 paleoclimate to hydrothermal. SEPM special publication, Thermal History Analysis of
581 Sedimentary Basins, 31 103, 45-63.
582 Goldstein, R.H. and Reynolds, T.J. (1994) Systematics of fluid inclusions in diagenetic
583 minerals: SEPM Short Course Notes, 31. 199.
584 Hao, F., Guo, T.L., Zhu, Y.M., Cai, X.Y., Zou, H.Y. and Li, P.P. (2008) Evidence for
585 multiple stages of oil cracking and thermochemical sulfate reduction in the Puguang
586 gas field, Sichuan Basin, China. American Association of Petroleum Geologists,
587 Bulletin 92, 611.
588 Hao, F., Zhang, X.F., Wang, C.W., Li, P.P., Guo, T.L., Zou, H.Y., Zhu, Y.M., Liu, J.Z. and
589 Cai, Z.X. (2015) The fate of CO2 derived from thermochemical sulfate reduction (TSR)
590 and effect of TSR on carbonate porosity and permeability, Sichuan Basin, China.
591 Earth-Science Reviews 141, 154-177.
592 Heydari, E. (1997) The role of burial diagenesis in hydrocarbon destruction and H2S
593 accumulation, Upper Jurassic Smackover Formation, Black Creek Field, Mississippi.
594 American Association of Petroleum Geologists, Bulletin 81, 26-45.
595 Heydari, E. (2000) Porosity loss, fluid flow, and mass transfer in limestone reservoirs:
596 Application to the upper Jurassic Smackover formation, Mississippi. American
597 Association of Petroleum Geologists, Bulletin 84, 100-118.
598 Huang, S.J., Huang, K.K., Lü, J. and Lan, Y.F. (2012) Carbon isotopic composition of Early
599 Triassic marine carbonates, Eastern Sichuan Basin, China. Science China Earth
600 Sciences 55, 2026-2038.
601 Hutcheon, I. and Krouse, H.R. (1994) Thermochemical sulfate reduction, evidence from the
602 field, theory and experiment. Abstracts of Papers of the American Chemical Society
603 208, 105-GEOC.
604 Hutcheon, I., Krouse, H.R. and Abercrombie, H.J. (1995) Controls on the origin and
605 distribution of elemental sulfur, H_2S, and CO_2 in paleozoic hydrocarbon reservoirs in
606 Western Canada, in: Vairavamurthy, M.A., Schoonen, M.A.A. (Eds.), Geochemical
607 Transformations of Sedimentary Sulfur, pp. 426-438.
608 Jiang, L., Cai, C., Worden, R., Li, K.K. and Xiang, L. (2013) Reflux dolomitization of the
609 Upper Permian Changxing Formation and the Lower Triassic Feixianguan Formation,
610 NE Sichuan Basin, China. Geofluids.
611 Jiang, L., Cai, C.F., Worden, R.H., Crowley, S.F., Jia, L.Q., Zhang, K. and Duncan, I.J. (2016)
612 Multiphase dolomitization of deeply buried Cambrian petroleum reservoirs, Tarim
613 Basin, north-west China. Sedimentology 63, 2130-2157.
614 Jiang, L., Cai, C.F., Worden, R.H., Li, K.K., Xiang, L., Chu, X.L., Shen, A.J. and Li, W.J.
615 (2015a) Rare earth element and yttrium (REY) geochemistry in carbonate reservoirs
616 during deep burial diagenesis: Implications for REY mobility during thermochemical
617 sulfate reduction. Chemical Geology 415, 87-101.
618 Jiang, L., Pan, W.Q., Cai, C.F., Jia, L.Q., Pan, L.Y., Wang, T.K., Li, H.X., Chen, S.L. and
619 Chen, Y. (2015b) Fluid mixing induced by hydrothermal activity in the Ordovician
620 carbonates in Tarim Basin, China. Geofluids.
621 Jiang, L., Worden, R.H. and Cai, C.F. (2014a) Thermochemical sulfate reduction and fluid
622 evolution of the Lower Triassic Feixianguan Formation sour gas reservoirs, northeast
623 Sichuan Basin, China. American Association of Petroleum Geologists, Bulletin 98,
624 947-973.
625 Jiang, L., Worden, R.H. and Cai, C.F. (2015c) Generation of isotopically and compositionally
626 distinct water during thermochemical sulfate reduction (TSR) in carbonate reservoirs:

627 Triassic Feixianguan Formation, Sichuan Basin, China. Geochimica et Cosmochimica
628 Acta 165, 249-262.
629 Jiang, L., Worden, R.H., Cai, C.F., Li, K.K., Xiang, L., Cai, L.L. and He, X.Y. (2014b)
630 Dolomitization of Gas Reservoirs: The Upper Permian Changxing and Lower Triassic
631 Feixianguan Formations, Northeast Sichuan Basin, China. Journal of Sedimentary
632 Research 84, 792-815.
633 Kenter, J.A.M., Harris, P.M., Collins, J.F., Weber, L.J., Kuanysheva, G. and Fischer, D.J.
634 (2006) Late Visean to Bashkirian platform cyclicity in the central Tengiz buildup,
635 Precaspian Basin, Kazakhstan: Depositional evolution and reservoir development, in P.
636 M. Harris and L. J. Weber, eds., Giant hydrocarbon reservoirs of the world: From rocks
637 to reservoir characterization and modeling: . AAPG Memoir 88, SEPM Special
638 Publication, 7-54.
639 Krouse, H.R., Viau, C.A., Eliuk, L.S., Ueda, A. and Halas, S. (1988) Chemical and isotopic
640 evidence of thermochemical sulfate reduction by light hydrocarbon gases in deep
641 carbonate reservoirs. Nature 333, 415-419.
642 Kuo, C.H. (1972) On the production of hydrogen sulfide-sulfur mixtures from deep
643 formations. Journal of Petroleum Technology 24, 1,142-141,146.
644 Li, J., Xie, Z., Dai, J., Zhang, S., Zhu, G. and Liu, Z. (2005) Geochemistry and origin of sour
645 gas accumulations in the northeastern Sichuan Basin, SW China. Organic
646 Geochemistry 36, 1703-1716.
647 Lin, F., Bodnar, R. and Becker, S. (2007) Experimental determination of the Raman CH4
648 symmetric stretching (v1) band position from 1–650bar and 0.3–22° C: Application to
649 fluid inclusion studies. Geochimica et Cosmochimica Acta 71, 3746-3756.
650 Liu, D.H., Dai, J.X., Xiao, X.M., Tian, H., Yang, C., Hu, A.P., Mi, J. and Song, Z.G. (2009)
651 High density methane inclusions in Puguang Gasfield: Discovery and a TP genetic
652 study. Chinese Science Bulletin 54, 4714-4723.
653 Liu, D.H., Xiao, X.M., Xiong, Y.Q., Geng, A.S., Tian, H., Peng, P., Shen, J.G. and Wang,
654 Y.P. (2006) Origin of natural sulphur-bearing immiscible inclusions and H_2S in oolite
655 gas reservoir, Eastern Sichuan. Science in China Series D-Earth Sciences 49, 242-257.
656 Liu, Q.Y., Worden, R.H., Jin, Z.J., Liu, W.H., Li, J., Gao, B., Zhang, D.W., Hu, A.P. and
657 Yang, C. (2013) TSR versus non-TSR processes and their impact on gas geochemistry
658 and carbon stable isotopes in Carboniferous, Permian and Lower Triassic marine
659 carbonate gas reservoirs in the Eastern Sichuan Basin, China. Geochimica et
660 Cosmochimica Acta 100, 96-115.
661 Liu, Q.Y., Worden, R.H., Jin, Z.J., Liu, W.H., Li, J., Gao, B., Zhang, D.W., Hu, A.P. and
662 Yang, C. (2014) Thermochemical sulphate reduction (TSR) versus maturation and their
663 effects on hydrogen stable isotopes of very dry alkane gases. Geochimica et
664 Cosmochimica Acta 137, 208-220.
665 Liu, Y.F., Qiu, N.S., Xie, Z.Y., Yao, Q.Y. and Zhu, C.Q. (2016) Overpressure compartments
666 in the central paleo-uplift, Sichuan Basin, southwest China. AAPG Bulletin 100, 867-
667 888.
668 Loucks, R.G. (1999) Paleocave carbonate reservoirs; origins, burial-depth modifications,
669 spatial complexity, and reservoir implications. American Association of Petroleum
670 Geologists, Bulletin 83, 1795-1834.
671 Lucia, F.J., Major, R.P., Purser, B., Tucker, M. and Zenger, D. (1994) Porosity evolution
672 through hypersaline reflux dolomitization. Dolomites: A Volume in Honour of
673 Dolomieu 21.
674 Ma, Y.S., Guo, T.L., Zhao, X.F. and Cai, X.Y. (2008a) The formation mechanism of high-
675 quality dolomite reservoir in the deep of Puguang Gas Field. Science in China Series
676 D-Earth Sciences 51, 53-64.
677 Ma, Y.S., Zhang, S., Guo, T.L., Zhu, G., Cai, X.Y. and Li, M. (2008b) Petroleum geology of
678 the Puguang sour gas field in the Sichuan Basin, SW China. Marine and Petroleum
679 Geology 25, 357-370.
680 Machel, H.G. (1987) Saddle dolomite as a by-product of chemical compaction and
681 thermochemical sulfate reduction. Geology 15, 936-940.

Machel, H.G. (2001) Bacterial and thermochemical sulfate reduction in diagenetic settings—old and new insights. Sedimentary Geology 140, 143-175.

Machel, H.G. and Buschkuehle, B.E. (2008) Diagenesis of the Devonian Southesk-Cairn Carbonate Complex, Alberta, Canada: Marine Cementation, Burial Dolomitization, Thermochemical Sulfate Reduction, Anhydritization, and Squeegee Fluid Flow. Journal of Sedimentary Research 78, 366.

Machel, H.G., Krouse, H.R., Riciputi, L.R. and Cole, D.R. (1995) Devonian Nisku sour gas play, Canada: A unique natural laboratory for study of thermochemical sulfate reduction, in: Vairavamurthy, M.A., Schoonen, M.A.A. (Eds.), Geochemical Transformations of Sedimentary Sulfur, pp. 439-454.

Mazzullo, S.J. and Harris, P.M. (1991) An overview of dissolution porosity development in the deep-burial environment, with examples from carbonate reservoirs in the Permian Basin. Permian Basin Plays¨CTomorrow¡¯s Technology Today: West Texas Geological Society, Publ, 125-138.

Mazzullo, S.J. and Harris, P.M. (1992) Mesogenetic dissolution: its role in porosity development in carbonate reservoirs (1). AAPG bulletin 76, 607-620.

Meyer, B. (1976) Elemental sulfur. Chemical Reviews 76, 367-388.

Oakes, C.S., Bodnar, R.J. and Simonson, J.M. (1990) The system NaCl□ CaCl 2□ H 2 O: I. The ice liquidus at 1 atm total pressure. Geochimica et Cosmochimica Acta 54, 603-610.

Packard, J.J., Al-Aasm, I., Samson, I., Berger, Z. and Davies, J. (2001) A Devonian hydrothermal chert reservoir: the 225 bcf Parkland field, British Columbia, Canada. American Association of Petroleum Geologists, Bulletin 85, 51-84.

Parkhurst, D.L. and Appelo, C.A.J. (2013) Description of input and examples for PHREEQC version 3—A computer program for speciation, batch-reaction, one-dimensional transport, and inverse geochemical calculations. US Geological Survey Techniques and Methods 6, 497.

Qiu, N.S., Qin, J.Z., McInnes, B., Wang, J. and Zhen, L.J. (2008) Tectonothermal evolution of the northeastern Sichuan Basin: Constraints from apatite and zircon (U-Th)/He ages and vitrinite reflectance data. Geol J Chin Univ 14, 223-230.

Saller, A.H. and Dickson, J.A.T.D. (2011) Partial dolomitization of a Pennsylvanian limestone buildup by hydrothermal fluids and its effect on reservoir quality and performance. American Association of Petroleum Geologists, Bulletin 95, 1745-1762.

Smith, L.B. (2006) Origin and reservoir characteristics of Upper Ordovician Trenton–Black River hydrothermal dolomite reservoirs in New York. American Association of Petroleum Geologists, Bulletin 90, 1691-1718.

Worden, R.H. and Smalley, P.C. (1996) H_2S-producing reactions in deep carbonate gas reservoirs: Khuff Formation, Abu Dhabi. Chemical geology 133, 157-171.

Worden, R.H., Smalley, P.C. and Cross, M.M. (2000) The influence of rock fabric and mineralogy on thermochemical sulfate reduction: Khuff Formation, Abu Dhabi. Journal of Sedimentary Research 70.

Worden, R.H., Smalley, P.C. and Oxtoby, N.H. (1995) Gas souring by thermochemical sulfate reduction at 140 degrees C. American Association of Petroleum Geologists Bulletin 79, 854-863.

Worden, R.H., Smalley, P.C. and Oxtoby, N.H. (1996) The effects of thermochemical sulfate reduction upon formation water salinity and oxygen isotopes in carbonate gas reservoirs. Geochimica et Cosmochimica Acta 60, 3925-3931.

Xu, T.F., Kharaka, Y.K., Doughty, C., Freifeld, B.M. and Daley, T.M. (2010) Reactive transport modeling to study changes in water chemistry induced by CO_2 injection at the Frio-I Brine Pilot. Chemical Geology 271, 153-164.

Yang, C., Hutcheon, I. and Krouse, H.R. (2001) Fluid inclusion and stable isotopic studies of thermochemical sulphate reduction from Burnt Timber and Crossfield East gas fields in Alberta, Canada. Bulletin of Canadian Petroleum Geology 49, 149-164.

Yang, C., Samper, J. and Montenegro, L. (2008) A coupled non-isothermal reactive transport model for long-term geochemical evolution of a HLW repository in clay. Environmental Geology 53, 1627-1638.

Zhao, W., Luo, P., Chen, G., Cao, H. and Zhang, B. (2005) Origin and reservoir rock characteristics of dolostones in the Early Triassic Feixianguan Formation, NE Sichuan Basin, China: Significance for future gas exploration. Journal of Petroleum Geology 28, 83-100.

Zhu, G.Y., Zhang, S.C., Liang, Y.B., Dai, J.X. and Li, J. (2005) Isotopic evidence of TSR origin for natural gas bearing high H_2S contents within the Feixianguan Formation of the northeastern Sichuan Basin, southwestern China. Science in China Series D-Earth Sciences 48, 1960-1971.

Zhu, G.Y., Zhang, S.C., Liang, Y.B., Ma, Y.S., Guo, T.L. and Zhou, G.Y. (2006) Distribution of high H_2S-bearing natural gas and evidence of TSR origin in the Sichuan basin. Acta Geologica Sinica 80, 1208-1218(In Chinese).

Table Caption

Table 1. Point counting data showing percentages of each component in TSR-prevailed dolo-grainstone reservoirs in the Feixiangian Formation

Table 2. Mineral volume and porosity change by TSR modeling, porosity before TSR.

Table 3. Permeability change by TSR modeling, the equation of relationship between porosity and permeability ($y = 0.0166e^{0.5498x}$, $R^2 = 0.6489$) was obtained from core plug measurement from the Luojia-2 well.

Figure Caption

Figure 1. (A) Location and main structural elements of the Sichuan Basin, modified from Hao et al. (2008). (B) Paleogeography and locations of the sampled gas fields in the Feixianguan Formation dolostone reservoirs.

Figure 2. Representative wells showing stratigraphic and porosity correlation of the ooid-enriched limestone (that has not experienced TSR) and dolostone (that experienced TSR) in the Feixianguan Formation. Dolostone that experienced TSR appears to have the better reservoir quality; modified from (Ma et al., 2008a).

Figure 3. Photomicrographs show TSR-related calcite and elemental sulphur in dissolution pores in the Feixianguan Formation. A) EDS image of calcite (white

colour in the pore space) with a small volume of elemental sulphur (green colour in the pore space) filling in dolomite host rock (red colour), from well D2, depth 4308 m. B) EDS image of elemental sulphur (green colour in the pore space) present around the dissolution enlarged pore spaces in dolomite host rock (red colour), from well LJ2, depth 3256.5 m; C) EDS image showing big elemental sulphur aggressive (green colour) and calcite cement (write colour) in dissolution enlarged pore, from well D2, depth 4308 m; D) BSEM image of elemental sulphur (red arrow) occurs as shield of dissolution enlarged pore, from well Du 4, depth 4793 m.

Figure 4. BESM images showing dissolution enlarged pore spaces and TSR-related calcite and pyrite in the Feixianguan Formation. A) Dissolution enlarged pore with size up to few millimetres locally filling with small volume of pyrite, well LJ 2, depth 3256.5 m. B) Dolo-grainstone enriched in dissolution enlarged pores with few calcite cements, well LJ 2, depth 3256.5 m. C) Dolostone reservoir containing open dissolution-enlarged pore spaces and a lack of cementation, well LJ 3-58. D) Intensive calcite cementation is observed in the left side of the image, whereas abundant dissolution enlarged pores present in the right side, from well Du 4, depth 4793 m.

Figure 5: BSEM images showing the protection of pore spaces by elemental sulphur and the dissolution of late stage dolomite in the Feixianguan Formation. A) Elemental sulphur (red arrow) occurs as a shield around the dolomite cements and host rock in an open pore, from well LJ 2, depth 3232.2 m. B) Elemental sulphur (red arrow) grow on the edge of an open pore, from well Po 2. C) Calcite precipitated in pore spaces that are lacking in elemental sulphur, pore spaces appear to be well-developed where elemental sulphur is present, from well Du 4, depth 4793 m. D) Late stage, pore-filling dolomite cement showing evidence of dissolution demonstrates that mesogenetic dissolution occurred during deep burial diagenetic environments, from well LJ 3-58.

Figure 6: Comparison of salinity and temperature from fluids inclusions in of oil-stage and gas-stage TSR calcite. Salinity of the formation water decreased from approximately 25 wt. % to less than 10 wt. % during oil-stage TSR, and formation salinity continue to decrease from about 10 wt. % down to approximately 5 wt. % during gas-stage TSR.

Figure 7: (A) Trapping pressures of fluid inclusions in TSR calcite. (B) Trapping temperature plotted against calculated trapping fluid pressures of fluids inclusions in TSR calcite with the data split into samples that had oil-stage TSR (oil inclusions present) and ones that gas-stage TSR (no oil inclusions present).

Figure 1. (A) Location and main structural elements of the Sichuan Basin, modified from Hao et al. (2008). (B) Paleogeography and locations of the sampled gas fields in the Feixianguan Formation dolostone reservoirs.

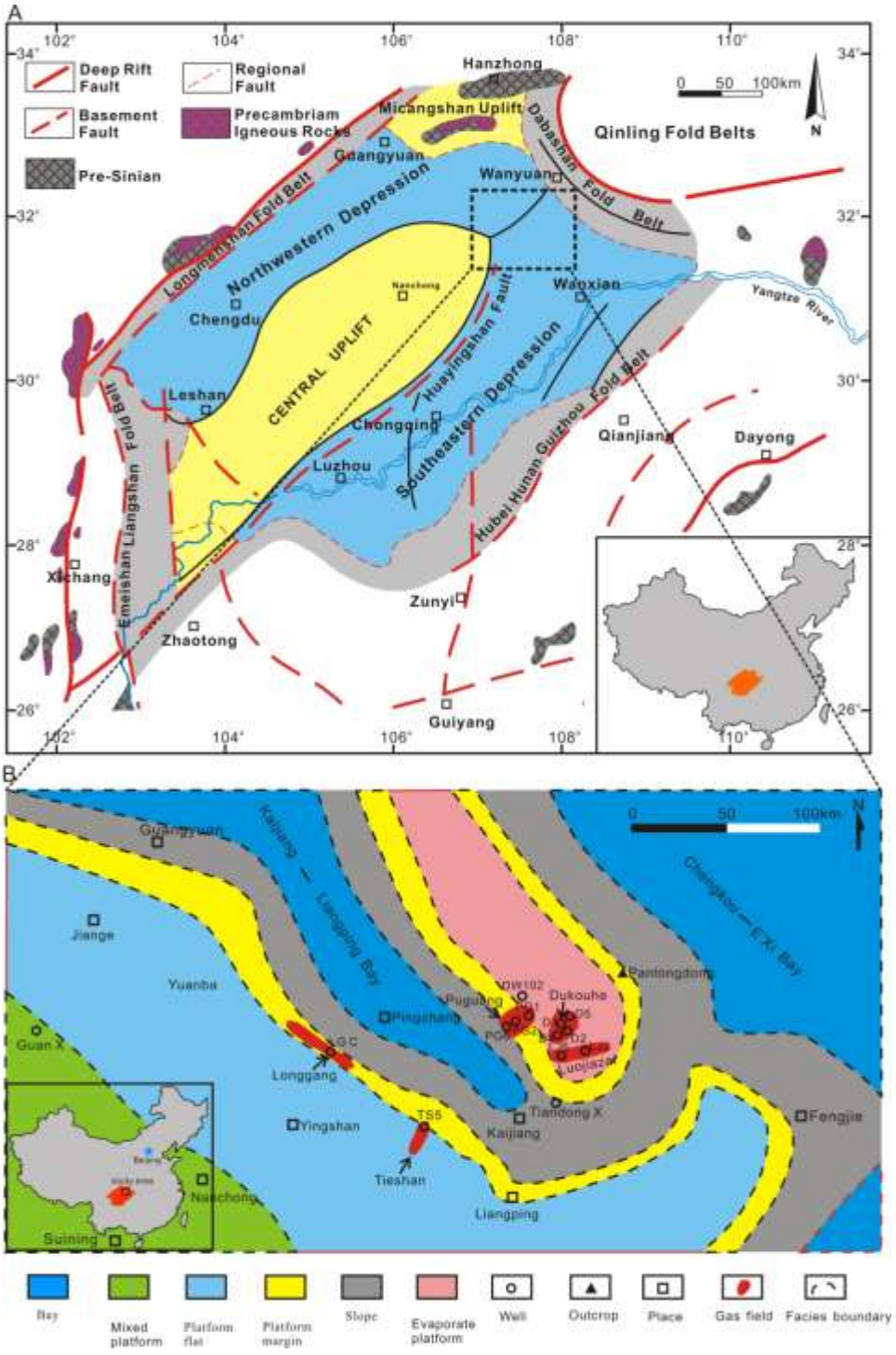

Figure 2. Representative wells showing stratigraphic and porosity correlation of the ooid-enriched limestone (that has not experienced TSR) and dolostone (that experienced TSR) in the Feixianguan Formation. Dolostone that experienced TSR appears to have the better reservoir quality; modified from (Ma et al., 2008a).

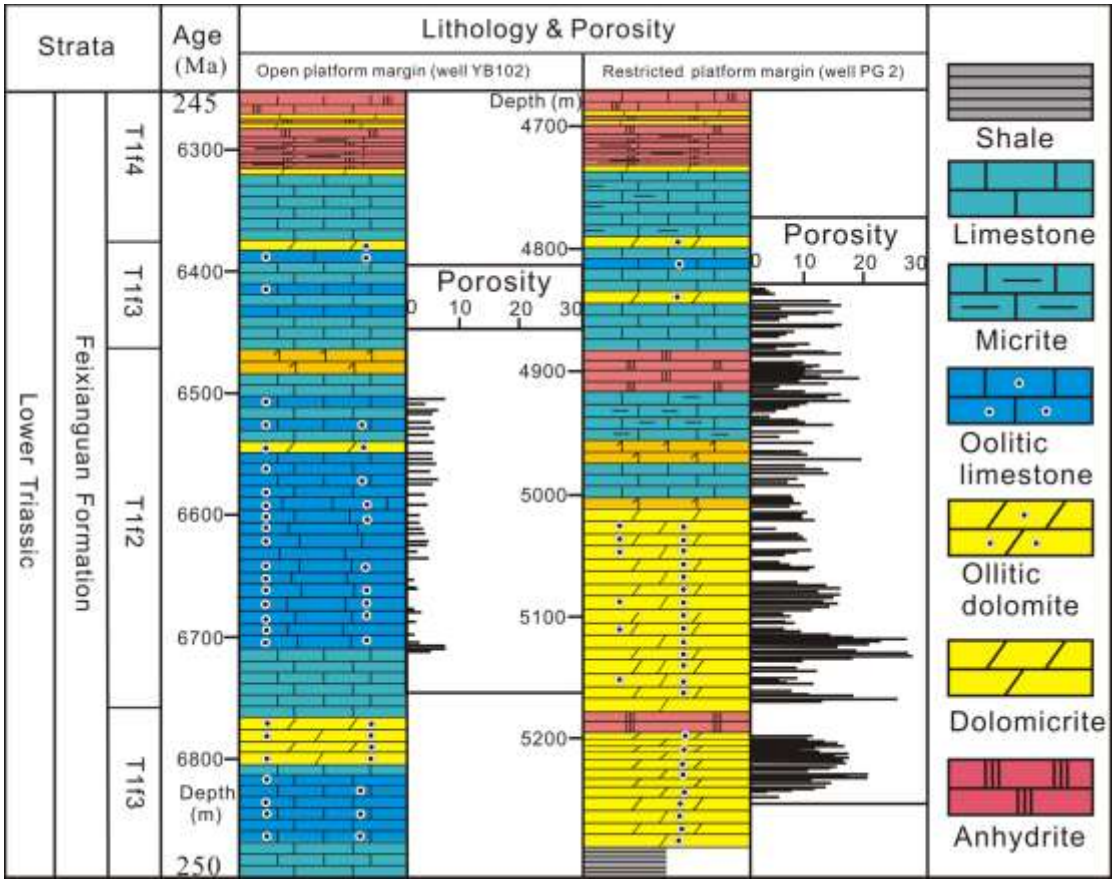

Figure 3. Photomicrographs show TSR-related calcite and elemental sulphur in dissolution pores in the Feixianguan Formation. A) EDS image of calcite (white colour in the pore space) with a small volume of elemental sulphur (green colour in the pore space) filling in dolomite host rock (red colour), from well D2, depth 4308 m. B) EDS image of elemental sulphur (green colour in the pore space) present around the dissolution enlarged pore spaces in dolomite host rock (red colour), from well LJ2, depth 3256.5 m; C) EDS image showing big elemental sulphur aggressive (green colour) and calcite cement (write colour) in dissolution enlarged pore, from well D2, depth 4308 m; D) BSEM image of elemental sulphur (red arrow) occurs as shield of dissolution enlarged pore, from well Du 4, depth 4793 m.

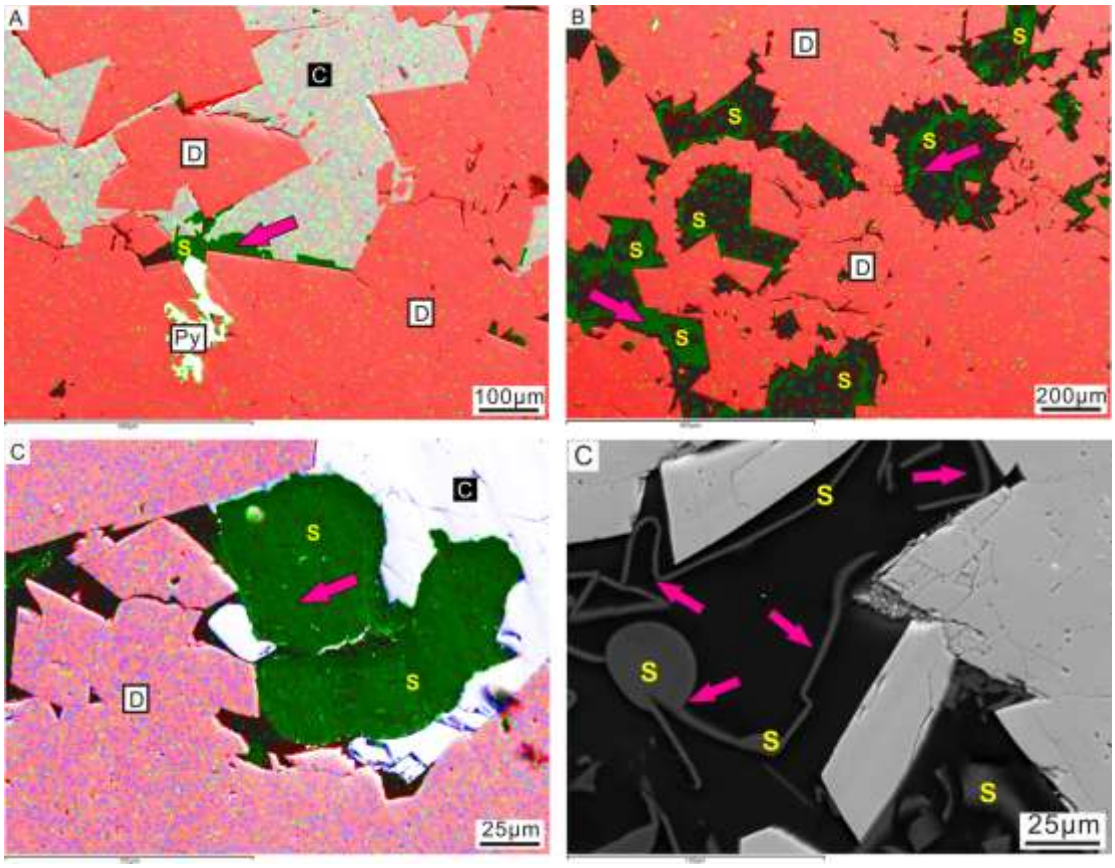

Figure 4. BESM images showing dissolution enlarged pore spaces and TSR-related calcite and pyrite in the Feixianguan Formation. A) Dissolution enlarged pore with size up to few millimetres locally filling with small volume of pyrite, well LJ 2, depth 3256.5 m. B) Dolo-grainstone enriched in dissolution enlarged pores with few calcite cements, well LJ 2, depth 3256.5 m. C) Dolostone reservoir containing open dissolution-enlarged pore spaces and a lack of cementation, well LJ 3-58. D) Intensive calcite cementation is observed in the left side of the image, whereas abundant dissolution enlarged pores present in the right side, from well Du 4, depth 4793 m.

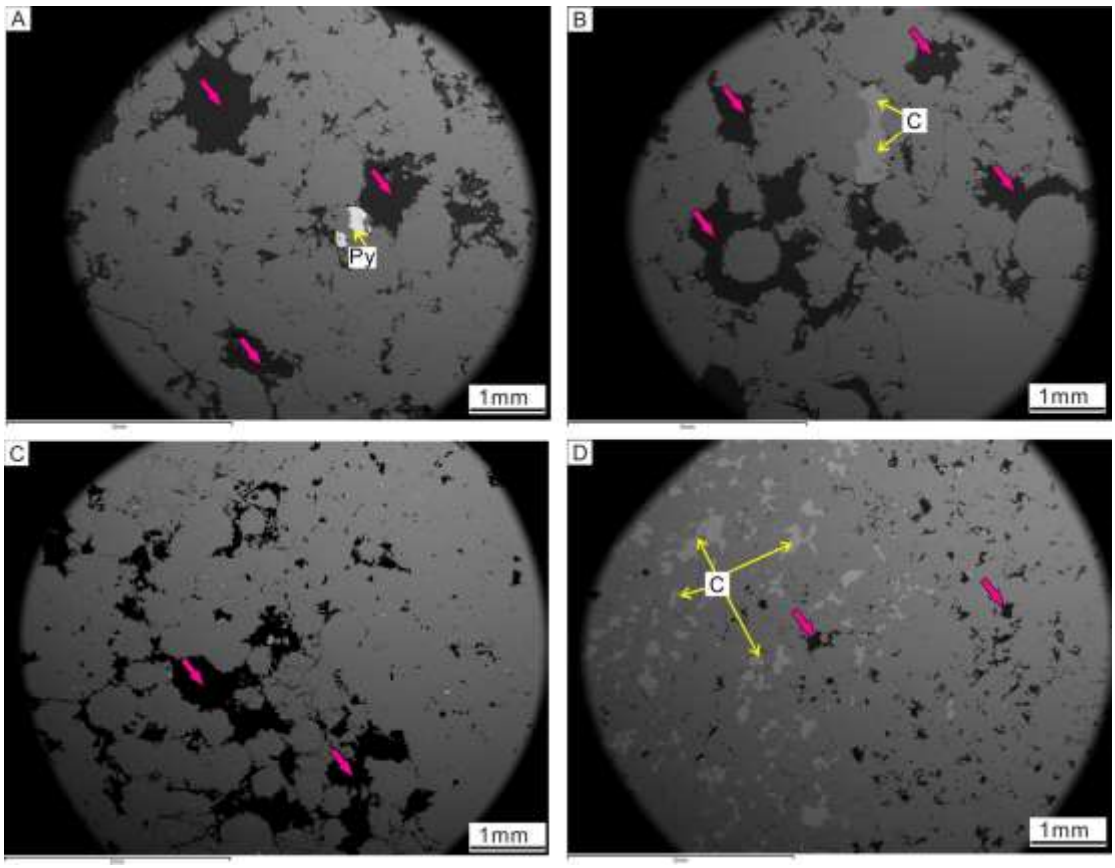

Figure 5: BSEM images showing the protection of pore spaces by elemental sulphur and the dissolution of late stage dolomite in the Feixianguan Formation. A) Elemental sulphur (red arrow) occurs as a shield around the dolomite cements and host rock in an open pore, from well LJ 2, depth 3232.2 m. B) Elemental sulphur (red arrow) grow on the edge of an open pore, from well Po 2. C) Calcite precipitated in pore spaces that are lacking in elemental sulphur, pore spaces appear to be well-developed where elemental sulphur is present, from well Du 4, depth 4793 m. D) Late stage, pore-filling dolomite cement showing evidence of dissolution demonstrates that mesogenetic dissolution occurred during deep burial diagenetic environments, from well LJ 3-58.

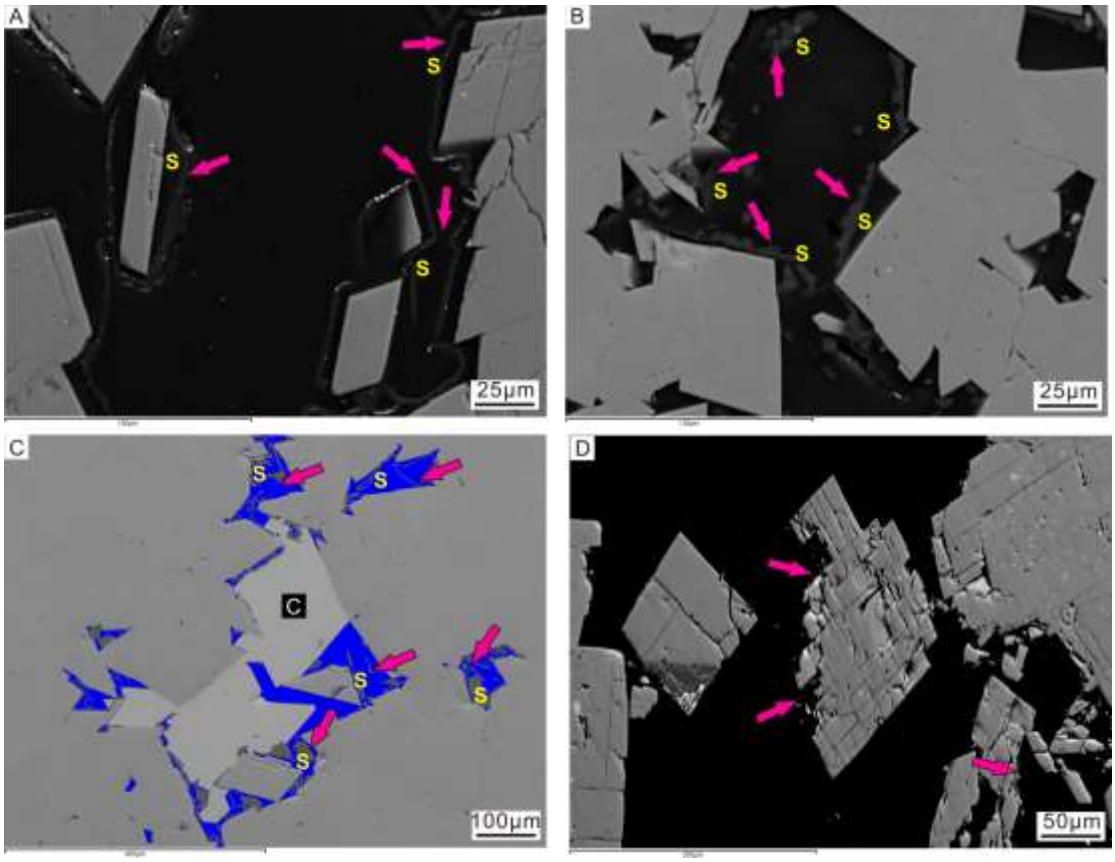

860 Figure 6: Comparison of salinity and temperature from fluids inclusions in of oil-stage
861 and gas-stage TSR calcite. Salinity of the formation water decreased from
862 approximately 25 wt. % to less than 10 wt. % during oil-stage TSR, and formation
863 salinity continue to decrease from about 10 wt. % down to approximately 5 wt. %
864 during gas-stage TSR.

865

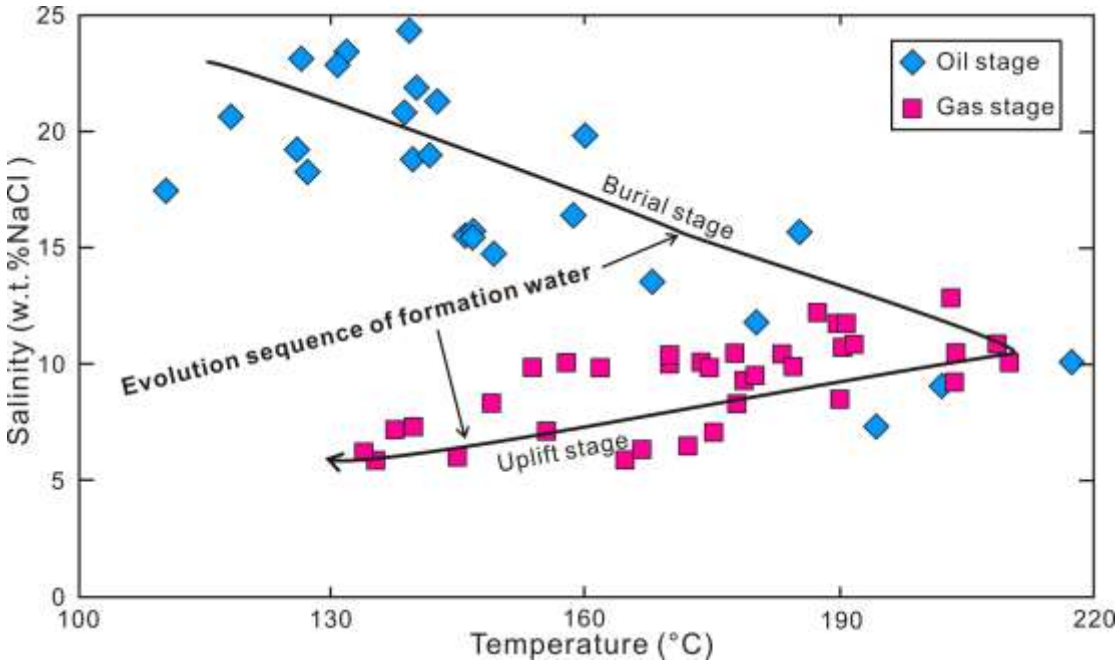

866

Figure 7: (A) Trapping pressures of fluid inclusions in TSR calcite. (B) Trapping temperature plotted against calculated trapping fluid pressures of fluids inclusions in TSR calcite with the data split into samples that had oil-stage TSR (oil inclusions present) and ones that gas-stage TSR (no oil inclusions present).

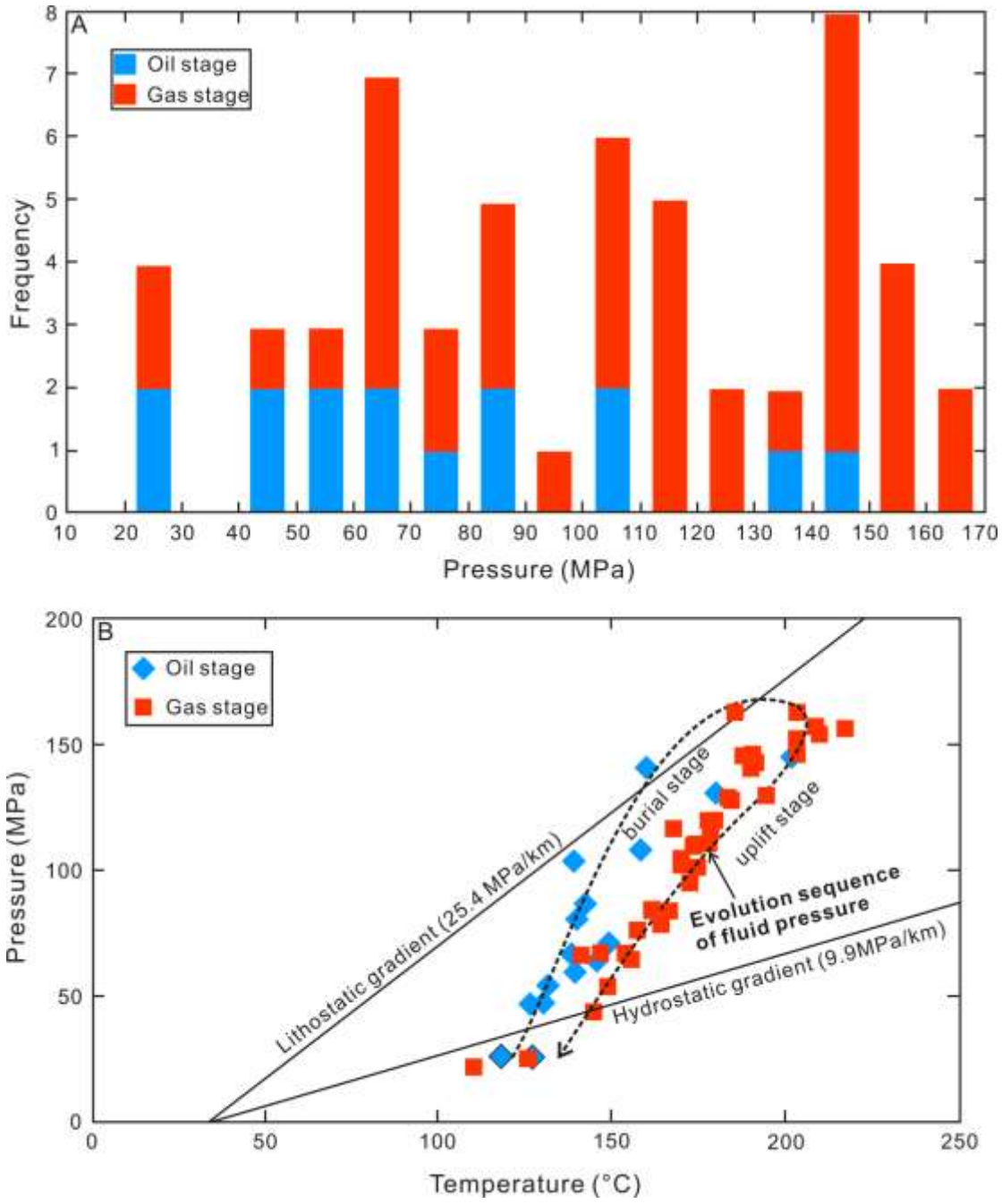

874 Table 1.

Sample No.	Depth (m)	Grain (%)	Matrix (%)	Carbonate cements (%)					Porosity (%)	Bitumen (%)	Pyrite (%)	Quartz (%)
				C1	C2	C3	D1	D2				
LJ2-1	3198	67	6	0	0	2	7	2	6	9	0	1
LJ2-18	3267	70	0	0	0	0	15	8	5	2	0	0
LJ2-25	3256	65	0	0	0	0	15	5	8	5	2	0
LJ2-33	3232	75	0	0	0	0	0	15	8	2	0	0
LJ2-37	3233	56	0	0	4	0	17	0	20	3	0	0
LJ2-26	3256	71	0	0	0	0	0	17	8	1	3	0
LJ3-58	--	69	0	0	2	0	10	5	13	0	1	0
LJ3-27	--	66	0	0	0	0	18	7	3	6	0	0
LJ2	--	71	0	0	2	0	8	15	2	1	1	0
LJ2-23	--	67	0	0	0	0	25	0	3	5	0	0
D1	--	58	0	0	3	0	17	4	9	8	0	1
D2-25	4309	62	0	0	5	0	0	20	10	1	2	0
D2-7	--	57	0	0	0	0	0	18	16	2	2	5
D4-4	4236	78	0	0	4	0	5	0	13	0	0	0
D5	4793	55	0	0	3	0	11	6	12	9	0	4
DW102	4901	71	9	17	3	0	0	0	0	0	0	0
PLD-3	outcrop	80	0	0	0	6	0	0	0	12	2	0
PLD-4	outcrop	72	0	0	0	14	0	0	0	14	0	0
LJ6-7	3936	65	0	0	0	0	12	8	8	7	0	0
PG1a	--	70	0	0	0	0	12	0	17	1	0	0
PG1b	--	72	0	0	0	0	5	5	17	1	0	0
PG2-24	5020	63	0	0	0	0	10	0	27	0	0	0
PG2-21	4987	60	0	0	0	0	0	14	25	1	0	0
PG2-20a	4978	83	0	0	0	0	12	0	3	2	0	0
PG2-27	5043	75	0	0	0	0	18	0	5	2	0	0
PG2-31	5076	72	0	0	0	0	5	20	0	3	0	0
PG2-32	5085	74	0	0	0	0	7	14	3	2	0	0
PG2-41	5196	70	0	0	0	0	13	5	10	2	0	0
PG2-39	5166	65	0	0	0	0	10	8	17	0	0	0
PG2-22a	4980	64	0	0	0	0	0	20	14	2	0	0
PG2-26	4937	75	0	0	0	0	13	0	12	0	0	0
PG2-21	4934	80	0	0	6	0	0	7	7	0	0	0
PG2-22b	4935	64	0	0	17	0	0	15	0	4	0	0

PG2-5	4776	67	0	0	14	0	0	5	13	0	0	1
PG2-20b	4982	38	0	0	0	0	12	17	33	0	0	0
PG2-30	5066	87	0	0	0	0	0	0	12	1	0	0
PG6-a	--	60	0	0	0	0	18	7	10	5	0	0
PG6-b	--	68	0	0	0	0	0	0	2	26	4	0
PG6-c	5142	75	0	0	0	0	0	18	5	2	0	0
TS 5-9	--	66	0	0	3	0	14	0	6	11	0	0
TS 5-11	--	56	0	0	0	0	14	0	18	12	0	0
TS 5-12	--	49	0	0	1	0	24	0	10	16	0	0
TS 5-13	--	53	18	0	2	0	14	0	2	11	0	0
LGC	5933	65	0	0	3	0	17	0	13	2	0	0
Average value		67.0	0.8	0.4	1.6	0.5	8.6	6.5	9.7	4.4	0.4	0.3

875 -- data unavailable; C1: Pre-TSR calcite; C2: TSR calcite; C3: Post-TSR calcite; D1: Early reflux
876 dolomite; D2: late burial dolomite

877

878 Table 2.

	Minerals	Initial volume before TSR (cm^3)	Final volume after TSR (cm^3)	Relative porosity change (%)	Net porosity change（%）
Case 1 16% porosity	Anhydrite	505	0.0	-6.00	-5.0
	Calcite	84	428	4.1	3.4
	Dolomite	7811	7811	0.0	0.0
	Total	8400	8239	-1.92	-1.6
Case 2 10% porosity	Anhydrite	541	0.0	-6.00	-5.4
	Calcite	90	459	4.1	3.7
	Dolomite	8369	8369	0.0	0.0
	Total	9000	8830	-2.06	-1.7

879

880

881 Table 3.

	Initial Porosity before TSR (%)	Final Porosity after TSR (%)	Initial Permeability before TSR (mD)	Final Permeability before TSR (mD)
Case 1	16	17.6	109.7	264.3
Case 2	10	11.7	4.1	10.3

882

883